DOI link to article:

http://dx.doi.org/10.1039/C5DT02191J

Date deposited:

28/07/2015

Embargo release date:

20 July 2016

The Ferrocene Effect: Enhanced Electrocatalytic Hydrogen Production using meso-Tetraferrocenyl porphyrin Palladium (II) and Copper (II) Complexes

D. Sirbu,[a] C. Turta,[a] E. A. Gibson[b*] and A. C. Benniston[b*]

Copper(II) and palladium(II) *meso*-tetraferrocenylporphyrins (**CuTFcP** and **PdTFcP**) were employed as catalysts for electrochemical proton reduction in DMF using trifluoroacetic acid (TFA) or triethylamine hydrochloride (TEAHCl) as acids. Gas analysis under electrocatalytic conditions at a glassy carbon working electrode confirmed the product as H_2. **CuTFcP** showed catalytic behavior for both TFA and TEAHCl, whereas only TFA worked for **PdTFcP**. The performance of the two compounds for electrocatalytic hydrogen generation was compared to the analogous copper(II) and palladium(II) *meso*-tetraphenylporphyrins (**CuTPP** and **PdTPP**) under identical conditions. The presence of the ferrocence groups on the porphyrin favourably shift the overpotential to a less negative value by around 200 mV and increases the catalytic rate of hydrogen production in DMF/TFA by an order of magnitude to 6×10^3 s^{-1}. Moreover, while **CuTPP** is fully inactive in a DMF/TEAHCl mixture, the ferrocene subunits activate the **CuTFcP** catalyst. Spectroelectrochemistry experiments and DFT calculations were consistent with a catalytic process proceeding via the phlorin anion.

Introduction

A facile and readily controllable method for the production of hydrogen gas by the reduction of protons offers a way to generate a highly combustible fuel or feedstock for chemical reactions.[1,2] Even though the electrolysis of water for hydrogen generation is a well-established technology, and hydrogen is frequently cited as a "clean fuel", it has yet to be adopted on a sizeable scale.[3] Large-scale fossil fuels combustion to generate the electricity required is counter productive, yet electrolysis offers a way of storing the energy from renewable sources to overcome problems with intermittent supply of e.g., wind and solar power.[4] However, there is a significant cost barrier to the widespread use of electrolysis to generate hydrogen rather than steam reforming. Much of this cost comes from the price of the electrode materials, which are usually based on precious metals, and the energy input required to split water.[5] Even though proton reduction at platinum is facile the scarcity of the metal has fuelled research efforts to develop cheaper and more abundant electrode materials.[6] One problem to overcome is the large overpotential that hampers the use of, for example, glassy carbon electrodes.[7] One solution to the problem is to employ electrocatalysts which are capable of lowering the overpotential to drive the two electron two proton reduction process.[8]

For some time transition metal porphyrins have been known for their applications in electrocatalysis including many industrially imperative reactions.[9] Particular attention has been paid to electrocatalytic reduction of carbon dioxide by metal (e.g., Ag(II), Pd(II), Co(II), Fe(0)) porphyrin derivatives.[10-12] Examples of electrochemical proton reduction catalysed by metal (e.g., Co(I), Fe(0)) porphyrin derivatives are also known,[13,14] however no examples are known for palladium(II) and copper (II) porphyrin complexes. In fact, to the best of our knowledge the only, and very recently reported, use of palladium complex catalysed hydrogen evolution was based mostly on cyclic voltammetry experiments and no detection of the electrolysis products was performed.[15] As was shown previously, ferrocene substituents can operate as electron donors for the four-electron reduction of O_2 by using an iron(III)(tetraferrocenyl)porphyrin; a triazole moiety acts as a bridge between the porphyrin and ferrocene groups and hydrogen bonding facilitates the proton transfer pathway towards the active site of the catalyst.[16] It was later shown that **CoTFcP** can be used for reduction of O_2 to H_2O_2 with high selectivity, probably by preventing catalyst dimerization by steric hindrance of the ferrocene units.[17] With this in mind we synthesized the palladium(II) (**PdTFcP**) and copper(II) (**CuTFcP**) tetraferrocenylporphyrin complexes (Figure 1), with the initial intention of focussing on electrocatalytic CO_2 reduction. Even though the compounds were found not to be active for this reaction, they did prove to be electrocatalysts for reducing protons to molecular hydrogen in the presence of either TFA or TEAHCl as a proton source. The main point to note is that the copper complex of tetraphenylporphyrin (**TPP**) was previously reported to be a non-active hydrogen evolving catalyst (with TEAHCl or CHF_2COOH),[14] and we found that both **CuTPP** and **PdTPP** are far less active than their ferrocene analogue when using TFA as the acid source. The appended ferrocene groups appear to be extremely important in enhancing the electrocatalytic process.
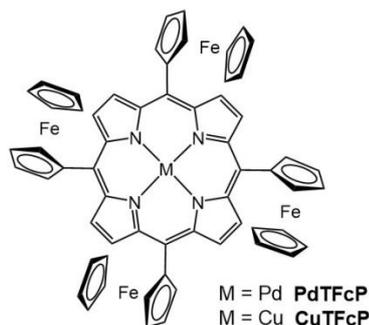

M = Pd **PdTFcP**
M = Cu **CuTFcP**

Results and discussion

Synthesis & Characterisation

The free-base tetraferrocenylporphyrin **H₂TFcP** was prepared by the standard literature procedure.[18,19] The copper(II) tetraferrocenylporphyrin **CuTFcP**[20] and the new palladium(II) derivative **PdTFcP** were obtained by complexation of the free-base tetraferrocenylporphyrin with copper(II) acetate or palladium(II) acetate in moderate yields (~20%). The requirement for careful chromatography purification is one reason for the low yields. The ¹H-NMR spectrum for **PdTFcP** (see ESI) showed a clear singlet for the β-protons at 9.67 ppm (8H) consistent with a symmetrical porphyrin, and two apparent triplets at 5.27 (8H) and 4.74 ppm (8H) together with a singlet at 3.98 ppm (20 H) typical for a mono-substituted ferrocene. The integration ratio for the proton signals of the ferrocene and porphyrin units is consistent with the structure. The incorporation of the palladium ion was confirmed by the loss of the NH signal (-0.5 ppm) associated with the free-base tetraferrocenyl porphyrin, and a cluster of peaks at *m/z* 1150 in the MALDI-TOF mass spectrum (see ESI) corresponding extremely well to the theoretical isotopic pattern. The presence of only one Q-band was also consistent with insertion of the palladium into the porphyrin ring. Mössbauer spectroscopy (see ESI) performed on **PdTFcP** and **CuTFcP** was consistent with the absence of any ferrocenium in the samples.
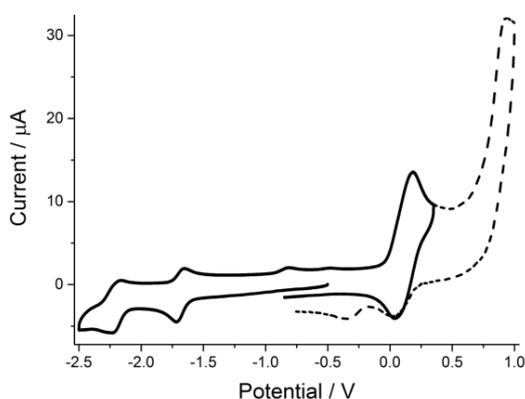
Cyclic Voltammetry

The redox behaviour of **PdTFcP** was studied by cyclic voltammetry in dried DMF and DCM using 0.2 M tetrabutylammonium tetrafluoroborate (TBATFB) as the supporting electrolyte to ensure the conductivity of the solution was adequate. The cyclic voltammogram in DMF consists of

redox patterns for a porphyrin and ferrocene moieties (Figure 2). Upon scanning to positive potentials a quasi-reversible wave at +0.08 V (vs. Fe(Cp)₂⁺/Fe(Cp)₂) is seen, which is associated with redox at the ferrocene sites. No splitting of the wave is evident but the peak's separation difference of 150 mV and magnitude of the peak current relative to the reduction waves would suggest that there are four overlapping waves. At a more positive potential an irreversible wave is observed at +0.93 V (vs. Fe(Cp)₂⁺/Fe(Cp)₂) and is a porphyrin-based oxidation process. The observed potential is shifted more positive when compared to other porphyrins, and is readily explained by the presence of the four ferrocenium ions which make the porphyrin more difficult to oxidize. Scanning to such a potential does not remove the reversibility of the ferrocene couple but it does give rise to a new wave at -0.38 V on the reverse sweep, which probably results from chemical modification of the generated cation. The reduction side of the voltammogram shows two quasi-reversible one-electron waves at -1.72 V and -2.21 V (vs. Fe(Cp)₂⁺/Fe(Cp)₂), and these are again associated with redox at the porphyrin site. The use of DCM as solvent results in several changes to the redox processes (see ESI). The reversibility of the first reduction wave is removed and shifted to a much more negative potential at -2.06 V (vs. Fe(Cp)₂⁺/Fe(Cp)₂). The second reduction wave cannot be observed as it is beyond the solvent potential window. The ferrocene is slightly easier to oxidize in DCM being shifted to -0.05 V (vs Fe(Cp)₂⁺/Fe(Cp)₂)), while the irreversible oxidation process on the porphyrin site is shifted to +1.05 V (vs Fe(Cp)₂⁺/Fe(Cp)₂)) and generates a comprehensive ferrocenium reduction wave. Presumably the low solubility of multi-charged species in DCM facilitates adsorption/desorption processes generating non-Faradaic currents. The electrochemistry of **CuTFcP** in DCM was described before.[21] The use of DMF as solvent gives a picture similar to the Pd analogue with four processes at -2.23, -1.70, +0.08 and +0.75 V (vs Fe(Cp)₂⁺/Fe(Cp)₂)) (see ESI).

UV-Visible Absorption Spectroscopy

The room temperature electronic absorption spectra for **H₂TFcP**, **CuTFcP** and **PdTFcP** in THF are shown in Figure 3 with the relevant parameters collated in Table 1. The spectra comprise of a strong Soret B-band and one weaker Q-band for the metalated porphyrins, while two Q-bands were found for **H₂TFcP**. The weak band at the high energy side of spectrum may be assigned to the porphyrin N-band. The Soret band also contains a shoulder in the region of ~500 nm which is ascribed by Nemykin *et al.*[22] to predominantly ferrocene-to-porphyrin charge transfer. The overall absorption of **PdTFcP** is weaker than its free metal and Cu(II) analogues, especially the Soret band which is more than twice reduced in intensity, while the Q-band is blue shifted compared to **CuTFcP**.
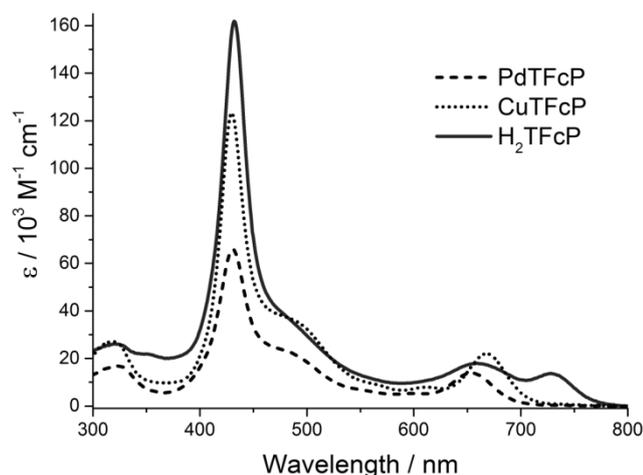
Figure 3. Room temperature UV-Visible absorption spectra for **H₂TFcP**, **CuTFcP** and **PdTFcP** in THF.

Table 1. UV-Visible absorption parameters for **H₂TFcP**, **CuTFcP** and **PdTFcP** in THF.

Compound	N-band, nm (ε, 10^3 M^{-1} cm^{-1})	Soret band, nm (ε, 10^3 M^{-1} cm^{-1})	Q-band, nm (ε, 10^3 M^{-1} cm^{-1})
H₂TFcP	321 (26)	432 (162)	660 (18) 728 (14)
CuTFcP	319 (27)	430 (123)	668 (22)
PdTFcP	324 (17)	431 (66)	654 (14)

UV-Visible Spectroelectrochemistry

Perturbation of the UV-Visible spectrum of **PdTFcP** was monitored using an optically transparent thin-layer electrode (OTTLE) and the spectroelectrochemistry method by application of negative and positive potentials. Application of a negative potential of -1.3 V to the working electrode produced a drastic decrease in the Soret band and the appearance of a red-shifted broad band. The Q-band almost fully disappeared and three new weak and broad bands appeared at 750, 875 and 1035 nm (Figure 4). The N-band is blue-shifted by 35 nm and there is a concomitant three-fold increase in its intensity. Similar behaviour of Soret band and appearance of near-IR bands were reported for reduction of **H₂TFcP** and its Zn(II), In(II) complexes, and were attributed to the porphyrin radical mono-anion **MTFcP$^{-\cdot}$** (M = metal, 2H).[23] It means that the first reduction process is porphyrin centered. Further reduction at -1.7 V resulted in a narrowing and slight decrease in the Soret band. In the low-energy side of the spectrum is witnessed a substantial increase in the absorption at 880 nm. There is also a slight increase in intensity of the N-band. The formation of the porphyrin dianion **MTFcP^{2-}** would result in disappearance of the near-IR bands, but a similar strong band at 825 nm was reported to correspond to the zinc(II) tetraphenylphlorin monoanion obtained both by chemical and electrochemical reduction of Zn(II) tetraphenylporphyrin.[24] A band at 830 nm for a metal free tetraphenylphlorin[25] has been also reported. It means that the second reduction results in formation of **MTFcP^{2-}** followed by rapid protonation to give the phlorin anion **MTFcPH$^{-\cdot}$**. Very similar results were obtained for the reduction of **CuTFcP** (see ESI), the main difference being the higher energy (807 nm) of the near-IR band and the lack of N-band.
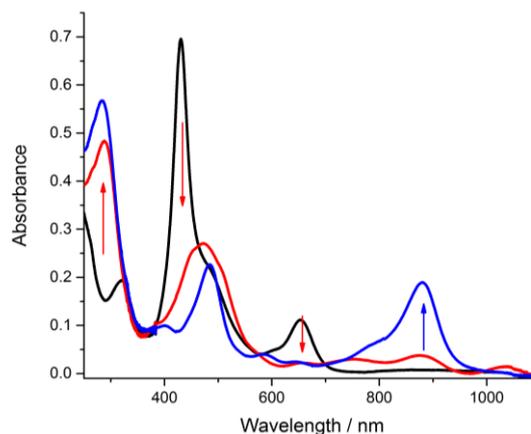

Figure 4. Electronic absorption spectra for **PdTFcP** in THF at the beginning (black) and after reduction at -1.3 V (red) and -1.7 V (blue) vs Ag wire.

Oxidation experiments were performed in DMF/THF mixture to avoid unwanted precipitation of the tetra-positive cation. Application of a potential at +0.9 V resulted in a decrease in intensity for the entire absorption profile (see ESI). It should be noted that the Soret band is slightly red-shifted and the low-energy shoulder completely disappears. No IVCT band was observed which confirms that all four ferrocenes were oxidized. The results are consistent with the work carried out by Nemykin and co-workers on metal-free and some transition metal ferrocene-porphyrins.[26] The alteration of absorption profile was fully reversible both in reduction and oxidation experiments.

Electrocatalysis

The addition of trifluoroacetic acid as a proton source to **PdTFcP** or **CuTFcP** gave rise to a new catalytic wave in the cyclic voltammograms at -2.0 V vs Fe(Cp)₂$^+$/Fe(Cp)₂ (estimated by using the "first derivative" technique).[27] The current response increased with further addition of acid, which was accompanied by a gradual shift of the peak maximum from -2.0 to -2.4 V. This is partially explained by the pH rise (Equation 1 from ESI), but formation of associates which are reduced at more negative potential is also possible. The form of the wave is representative of a diffusion limited process and is dependent on the acid concentration up to *ca*. 200 equivalents of TFA for **PdTFcP** (Figure 5) and 500 equivalents of TFA for **CuTFcP** (see ESI). A higher i_c/i_p ratio (where i_c is the current response of the catalytic wave and i_p is the current response of the sample in the absence of acid) for **CuTFcP** suggests an improved catalytic activity. The maximum turnover frequency (TOF$_{max}$) was estimated at *ca*. 6100 s^{-1}, and an overpotential of 1.0 − 1.2 V (Figure 6) was measured using methods described elsewere[27,28] (Eq.1 from ESI). The free-base, Zn(II) and Co(II) **TFcP** derivatives showed no catalytic activity under identical conditions, while Ni(II) **TFcP** generated a weak current response at a more negative potential. The use of the weaker acid triethylamine hydrochloride TEAHCl (pKa = 9.2) as the proton source resulted in no catalytic activity for **PdTFcP**, while **CuTFcP** showed similar behaviour as for TFA (see ESI). The presence of the copper(II) ion in the porphyrin ring is clearly more conducive for hydrogen

production, especially from weaker acids. The source of protons must be the acid as the catalysis does not occur in the absence of acid. No split of the wave is observed for an acid concentration up to 0.2 M, thus suggesting there are no significant competing parallel processes. However, at higher concentrations a shoulder is observed at the lower energy side of the catalytic peak at *ca*. -1.92 V vs Fe(Cp)$_2$$^+$/Fe(Cp)$_2$, and could be tentatively explained by the protonation of the porphyrin monoanion thus facilitating second reduction to form the phlorin ring. No change in the CV curve was observed when the Ar atmosphere was substituted with CO$_2$, in the presence or absence of TFA.

In order to elucidate the importance of the ferrocenyl groups for the proton reduction, Pd(II) tetraphenylporphyrin **PdTPP** was tested under similar conditions. Addition of TFA to the sample gave rise to a catalytic wave which is shifted to a more negative potential by ~200 mV as compared to **PdTFcP** (see ESI). The lower i$_c$/i$_p$ ratio at higher overpotential suggests a slower and more energy demanding catalysis by **PdTPP** as compared to the ferrocenyl analogue. The Cu(II) tetraphenyl porphyrin **CuTPP** analogue was reported by the Savéant group as being inactive for the catalysis of proton reduction in the presence of either TEAHCl or CHF$_2$COOH.[14] We repeated these experiments using TEAHCl and proved the lack of electrocatalytic response. Still, the use of TFA as proton source showed catalytic current response similar to **PdTPP** (see ESI). It stands out that introduction of ferrocenyl units in Cu(II) porphyrin opens up a way to the use of weaker acids, a very important effect in the attempt to use water as the proton source. It is noted that protons are reduced at much more negative potential (> 500 mV) on the glassy carbon surface in the absence of any catalyst, and a clear shift to a lower potential is observed when **CuTFcP** or **PdTFcP** catalyst is added to the solution, proving the catalytic effect (Figure 5).
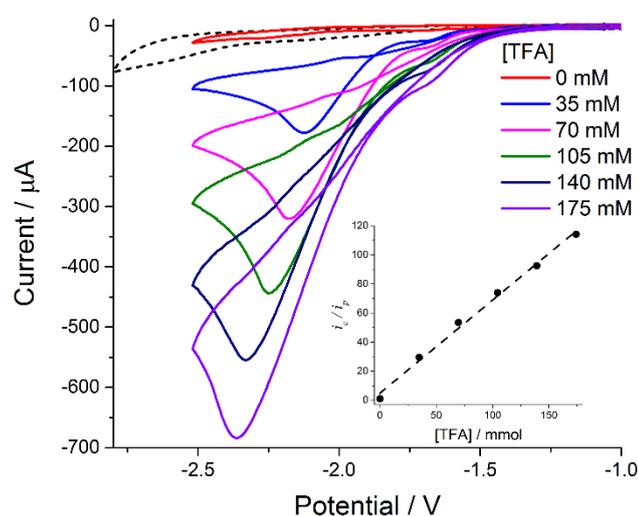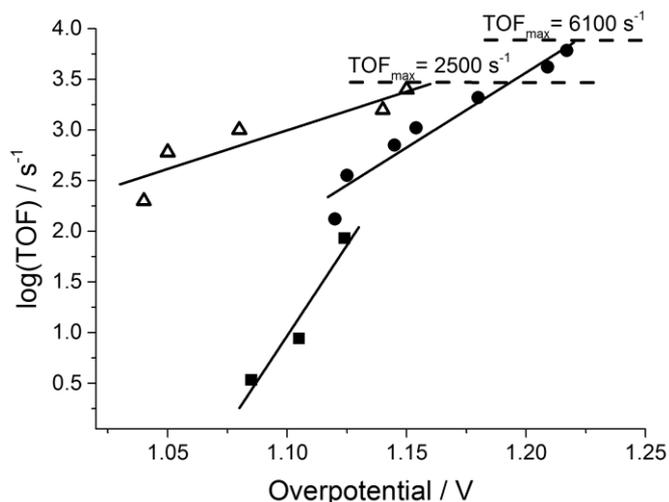

Figure 6. The TOF increase vs overpotential accompanying the addition of acid. The experimental points for: **PdTFcP** and TFA – triangles, **CuTFcP** and TFA – dots, **CuTFcP** and TEAHCl – squares. Solid line is showing the changes trend and dashed line is showing the maximum TOF at which catalytic current stops to increase with addition of acids.

Gas Analysis

A continuous flow-rig with in-line GC analysis was used to detect the molecular hydrogen produced during electrocatalytic proton reduction in DMF in the presence of TFA or TEAHCl.[29] It was found that applying a potential of -1.5 V vs saturated calomel electrode (SCE) at a glassy carbon working electrode resulted in the immediate formation of molecular hydrogen. The rate of H$_2$ produced was determined by calibration with a known flow rate of a H$_2$/Ar mixture by checking the proportionality between the peak area and the volume of injected hydrogen per minute. The presence of 0.1 mM of the catalysts greatly increased the rate of hydrogen produced as indicated by the GC analysis. Concomitantly an increase in the current response at the applied potential was noticed. Using 0.1 mM of **CuTFcP** in a DMF solution of 50 mM TFA with 0.2 M TBABF$_4$ as supporting electrolyte resulted in electrocatalytic production of H$_2$ with a 68 % Faradaic efficiency (Figure 7). A Faradaic efficiency of 70 % was obtained by the use of the **PdTFcP** catalyst (see ESI), but fewer protons were reduced in the same period of time consistent with a lower catalytic current response in the cyclic voltammetry experiments. For both compounds the current response during bulk electrolysis was constant for a period of at least one turnover cycle. On a prolonged timescale other Faradaic processes were noticed, and as result the glassy carbon electrode surface became modified resulting in an increase in the current response (see ESI). An explanation could be instability of ferrocene in the presence of TFA.[26,27]

Figure 5. Selected cyclic voltammograms for **PdTFcP** (1 mM) at a glassy carbon electrode in dry DMF in the presence of increasing quantities of TFA. Voltammograms show that the addition of acid leads to the appearance of an irreversible wave of increasing amplitude corresponding to the reduction of protons catalyzed by the complex. Conditions: T = 298 K, scan rate 100 mVs^{-1}. Supporting electrolyte: 0.2 M TBATFB. Dashed line shows the voltammogram for 35 mM solution of TFA in DMF in absence of any catalyst. Insert shows relationship between i$_c$/i$_p$ and concentration of acid.
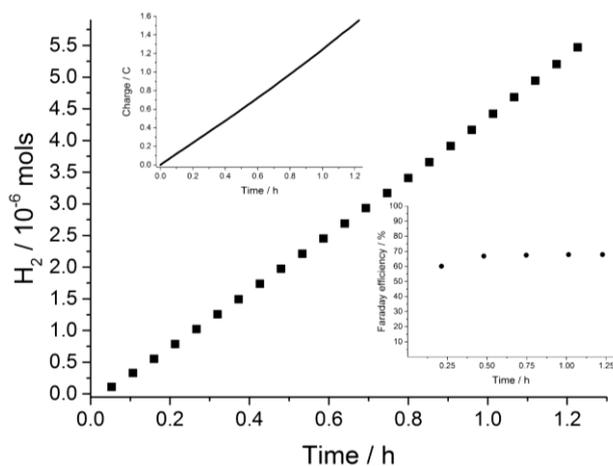
Figure 7. Electrocatalytic hydrogen production vs time, charge vs time (left top insert) and Faradaic efficiency vs time (right bottom insert) by applying -1.5 V vs SCE to a glassy carbon electrode in 0.2 M TBABF$_4$ solution of DMF containing 50 mM TFA and 0.1 mM **CuTFcP**.

As only **CuTFcP** showed electrocatalytic behaviour in the CV experiments when TEAHCl was employed as the proton source, it was used to generate H$_2$ from this weaker acid (Figure 8). As expected the catalysis process is slower for this acid at the same C_M = 50 mM, as result of the higher pKa = 9.2 (pKa = 6 for TFA).[28,30] A Faradaic efficiency of about 73 % was obtained. The decomposition process observed with TFA was absent when TEAHCl was used.
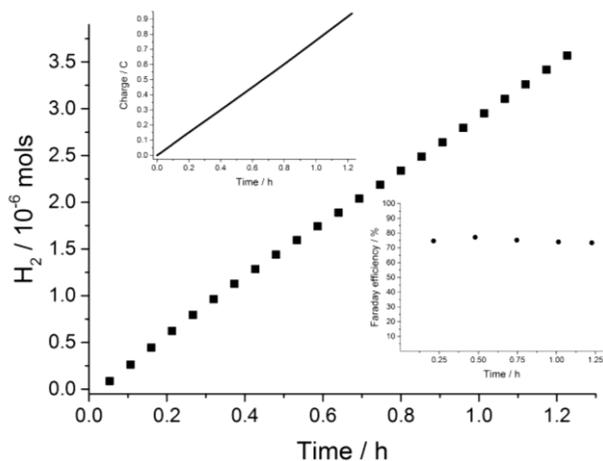
Computational and Mechanistic Considerations

The basic processes for electrocatalytic hydrogen production from metaloporphyrins (MP) are shown in Scheme 1. Prior work has delved into the mechanism in some detail focussing on the electrochemistry side and at which point in the cycle protonation takes place.[24,25,31] It is evident that both processes (a) and (b) depend on the pKa of the acid, the dianion (MP^{2-}) and its protonated form (MPH$^-$); process (c) is more likely kinetically

Figure 8. Electrocatalytic hydrogen production vs time, charge vs time (left top insert) and Faradaic efficiency vs time (right bottom insert) by applying -1.5 V vs SCE to a glassy carbon electrode in 0.2 M TBABF$_4$ solution of DMF containing 50 mM TEAHCl and 0.1 mM CuTFcP.

controlled. Addition of an electron to MP$^-$ is coupled to fast protonation and can be considered a proton-coupled electron transfer process.[32] As depicted in the scheme the reaction via the phlorin anion opens up a pathway to an intermediate after protonation where the aromaticity of a pyrrole is removed. A corollary is dehydrogenation would be favoured to re-aromatise the intermediate back to the porphyrin and thus act as a driving force for the reaction. It is worth stating that efficient hydrogen production from a highly stable phlorin anion is unfavored since it would be durable towards protonation. Formation of the chlorin is also possible within the mechanistic framework. The dominance of the intermediates is governed by the R groups (i.e., electron donating, bulkiness) and the metal ions (i.e., oxidation state, electronegativity). We were especially interested to determine the electron density distributions for MP, MP$^-$ and MP^{2-} and the orbitals contributions to see if there were major differences between the **PdTPP** and **PdTFcP** cases.
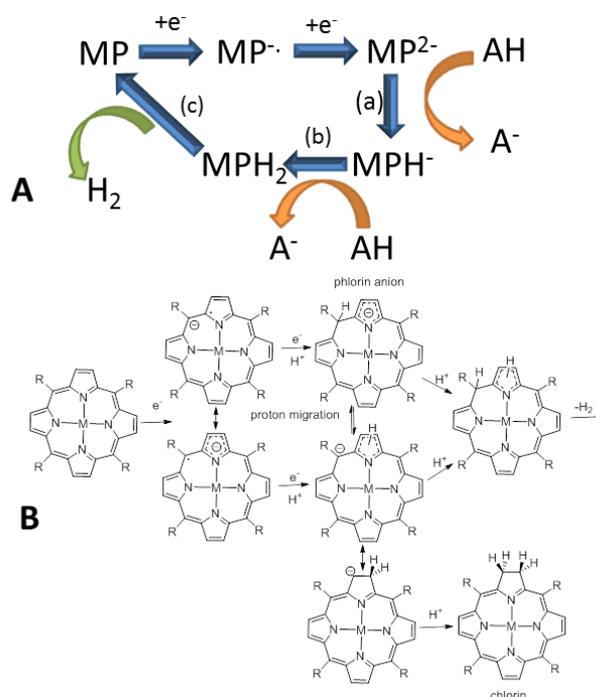
Scheme 1. (A) Simplified diagram showing the electrocatalytic formation of hydrogen from a metaloporphyrin (MP). (B) Potential products from the series of reduction and protonation processes. Note: at high concentration of acid the first protonation could take place at the porphyrin monoanion.

A somehow related scheme was recently proposed by Kadish *et al.* for explanation of the electrochemically initiated mechanisms leading to dehydrogenation of diprotonated porphyrins, but in this case the protonation occurs at the initial step.[33] The UV-Vis spectra for **CuTFcP** and **PdTFcP** did not change upon addition of TEAHCl or TFA, meaning that the protonation takes place at a later stage. At the same time, the first wave did not change upon addition of TEAHCl or TFA, supporting the idea that protonation takes place on the singly or doubly reduced porphyrins.[30] The phlorin macrocycle is relatively stable (at least under spectroelectrochemical conditions), requiring further protonation for dehydrogenation

to reform parent porphyrin,[31] thus heterolytic pathway of hydrogen evolution is strongly supported.

Energy minimised structures for **PdTPP** and **PdTFcP** were calculated using the Perdew nonlocal correlation function (B3PW91) and a 3-21G* basis set in Gaussian 09.[34] The Fe-C bond lengths of the ferrocene groups and Pd-N bond lengths for the calculated structures were comparable to X-ray determined values (see ESI). Hence, there is confidence that the methodology is suitable for the molecular systems. Minimised structures were also calculated for the radical anion (doublet state) and dianion (singlet state) species. A comparison of the two computed structures are shown in Figure 9, highlighting dihedral angles at the *meso* positions. The porphyrin ring for **PdTPP** is almost planar, which is consistent with X-ray determined structures.[35,36] The large bulky ferrocene groups in **PdTFcP** distort the porphyrin ring which is evident from the calculated dihedral angles. The structural distortion at the *meso* site is more pronounced for the ferrocene derivative. For both compounds there are *meso* sites where the dihedral angles increase upon formation of the radical anion and dianion (Table 2). Noting that the *meso* carbon must re-hybridise from sp^2 to sp^3 to generate a phlorin-anion structure, the ferrocene derivative **PdTFcP** seems slightly more predisposed to facilitate the structural change. However, prior work by Hambright and Neta suggested that protonation at the *meso* position is actually hampered by bulky groups at the site, by preventing the bending required for the hybridisation change.[37]

Table 2. Comparison of dihedral angles for calculated structures as defined in Figure 9.

Compound	Dihedral Angles / °			
	Neutral	Radical Anion	Dianion	Ratio[a]
PdTFcP	-9.36	-10.52	-14.43	1.12(1.54)
	-8.59	-10.87	-15.29	1.27 (1.78)
	-0.39	-5.26	-6.63	13.5 (17.0)
	-6.87	-5.81	-6.92	0.85 (1.0)
PdTPP	0.89	2.19	6.45	2.46 (7.25)
	0.18	-0.28	0.69	1.56 (3.83)
	0.88	2.09	-0.15	2.38 (0.17)
	-2.56	-3.74	-12.16	1.46 (4.75)

[a]Comparison of dihedral angles for radical anion to neutral form and dianion to neutral form (bracket).

Figure 9. Computer calculated molecular structures for **PdTPP** (A) and **PdTFcP** (B) using the B3PW91 function and a 3-21G* basis set and the selected dihedral angles.
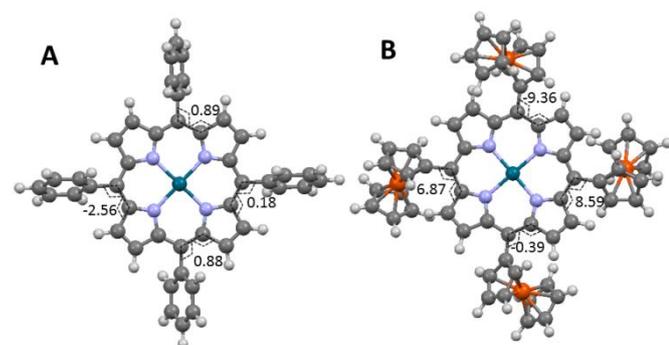
Despite the small difference in energies, the HOMOs for both **PdTPP** and **PdTFcP** are similar in appearance (Figure 10); major orbital contributions are associated with the *meso* carbons. In contrast, the energies for the LUMOs of the two derivatives are similar, but now there is a distinct difference in the molecular orbital picture. Firstly, a clear node is present for **PdTPP** which is not observed for the ferrocene derivative. In fact, there are distinct orbital contributions at each of the four *meso* carbons, affording a LUMO that is more evenly spread over the whole porphyrin unit. Similar energy-minimised structures and orbital pictures were generated for the radical anion and dianion (see ESI). One point to note from these calculations relates to the HOMOs and the single-occupied molecular orbitals (SOMOs) for the radical anion structures. The HOMO energies for **PdTPP**[-·] and **PdTFcP**[-·] are identical, but the SOMO for **PdTFcP**[-·] is around 230 mV lower in energy than the same orbital for **PdTPP**[-·]. That the predicted reduction potential for addition of an electron to **PdTFcP**[-·] should be more positive is consistent with the electrochemistry findings and in agreement with previous work by Nemykin *et al.,*[38] who found a gradual decrease by 160 mV for the second reduction potential by changing from mono-ferrocenyl to tetraferrocenyl free-base porphyrins. Molecular orbital pictures are very similar of the dianions for both compounds; orbital contributions at the four *meso* sites are prominent (see ESI). However, the newly formed HOMO for **PdTFcP**[2-] is more destabilised by *ca*. 330 mV compared to the phenyl analogue, in line with the electron donating capacity of the ferrocene groups. This difference in energy is probably not that important, although the HOMO is the site for protonation, since the reaction is fast for both catalysts.

Considering that prominent regions of high electron density are likely sites for protonation, the Mulliken charge (MC) distributions were also mapped out for the neutral, radical anion and dianion forms (see ESI). The results from these calculations are highlighted in Table 3. Two regions for the porphyrin ring are dominated by negative charge: the *meso* carbons and the β-pyrrole carbons. From the data presented in Table 3 it is evident that the electron donating ferrocence groups enhance negative charge at both sites for the neutral, radical anion and dianion species. Certainly worth noting is the prominent difference in MC between **PdTPP** and **PdTFcP** at the *meso* carbons for the dianion.
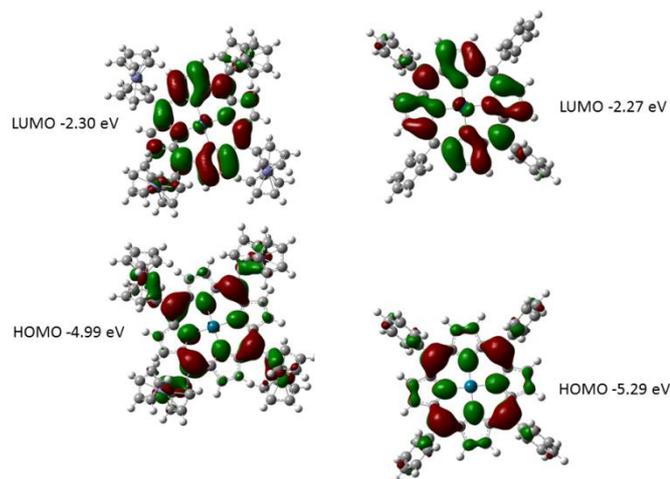

A   B

Figure 10. Computer calculated molecular orbitals for **PdTFcP** (left) and **PdTPP** (right) using the B3PW91 function and a 3-21G* basis set.

Table 3. Calculated Mulliken Charges (MC)[a] for the Palladium Porphyrins.

Form	Identity	**PdTPP**	**PdTFcP**	ΔMC[b]
Neutral	*meso* carbons	-0.505	-0.533	-0.028 (5.5%)[d]
	β-pyrrole carbons	-1.776	-1.940	-0.164 (9.2%)[d]
Radical anion	*meso* carbons	-0.548 (-0.043)[c]	-0.575 (7.9%)[c]	-0.027 (4.9%)[d]
	β-pyrrole carbons	-1.969 (-0.193)[c]	-2.108 (8.7%)[c]	-0.139 (7.1%)[d]
Dianion	*meso* carbons	-0.565 (-0.060)[c]	-0.615 (15.4%)[c]	-0.050 (8.8%)[d]
	β-pyrrole carbons	-2.129 (-0.353)[c]	-2.251 (16.0%)[c]	-0.122 (5.7%)[d]

[a] Mulliken charges given as the sum of the charges located at each carbon for the four *meso* carbons or eight *β*-pyrrole carbons. [b] Difference given as MC$_{PdTFcP}$-MC$_{PdTPP}$. [c] % difference between neutral form given in bracket. [d] Expressed as a percentage increase in bracket.

The spectroelectrochemistry experiments confirm that, unlike previous examples of metal-centered proton reduction catalysts, the reduction processes are porphyrin centred. It also appears that the porphyrin dianion MP^{2-} is protonated rapidly at the *meso* position to form the phlorin anion MPH$^-$. One out of four *meso* carbons is the probable protonation site for **CuTFcPH$^-$** and **PdTFcPH$^-$**, based on the computed orbital contributions and electron density at the carbon atoms. In contrast, only two sites are available for **MTPPH$^-$** (M = Cu^{2+}, Pd^{2+}). The phlorin anion is stable in THF under the spectroelectrochemical conditions, but the addition of a second proton is followed by H$_2$ evolution and regeneration of the catalyst. Certainly, it was previously shown that phlorins can undergo dehydrogenation in the presence of a proton source (HCl, MeOH) so that the parent porphyrin is regenerated.[31] The role played by the metal ion in the porphyrin ring is also worth mentioning. Highly electronegative metal ions (e.g., In^{3+}, Sn^{4+})[37,39] help stabilise the radical anion, which is long lived because of the inhibition to protonation. In addition, the ions also enhance the formation of the phlorin anion. The electronegativity of the copper(II) and palladium(II) ions appear

to be conducive to stabilise the negative charge at the pyrrole for the phlorin anion and thus disfavour resonance forms which would generate the chlorin.[40]

Conclusions

We have demonstrated that the attachment of the electron donating and bulky ferrocene groups to a metaloporphyrin can significantly enhance electrocatalytic hydrogen generation performance. Both steric and electronic effects likely contribute to enhanced operation of the catalysts. The overpotential is still too large for any practical application and the need to work in DMF is again not ideal. To shift the overpotential more positive, still using bulky ferrocene groups, seems feasible by functionalising the other cyclopentadienyl ring with a suitable electron withdrawing group. The carboxylate moiety may be suitable for such a purpose,[41] and in addition improve water solubility and serve as a site to promote proton-coupled electron transfer to the *meso* carbon.[42-44] We expect to test these ideas in new molecular electrocatalysts for hydrogen production.

Experimental

^{1}H- and ^{13}C- NMR spectra were recorded with Jeol ECS-400 MHz spectrometer. Chemical shifts are referenced relative to the residual protiated solvent. FT-Infrared spectra were recorded with a Varian 800 FT-IR spectrometer. MALDI-TOF experiments were conducted using Voyager DE-STR instrument with an Nd:YAG laser (λ = 355nm) by Elforlight. Electronic absorption spectra were recorded using a Hitachi U3310 spectrophotometer. [57]Fe-Mössbauer spectra were acquired at room temperature (RT) using a conventional spectrometer in the constant-acceleration mode (MS4, Edina, USA) equipped with a [57]Co source (3.7 GBq) in a rhodium matrix. Isomer shifts are given relative to α-Fe at RT. The spectrum was fitted using the Mössbauer Fitting Program (Edina). Cyclic voltammetry experiments were performed using Princeton Applied Research Potentiostat model 263a and a three electrode set-up consisting of a glassy carbon working electrode, a platinum wire counter electrode and an Ag/AgCl reference electrode. All studies were performed in deoxygenated DMF or DCM containing TBATFB (0.2 M) as background electrolyte. Redox potentials were reproducible to within ±15 mV. For spectroelectrochemical experiments platinum was used as working and counter electrodes and silver wire was used as a pseudoreference electrode. All potentials in cyclic voltammetry experiments are referenced vs ferrocene couple, while in the spectroelectrochemical experiments vs silver wire. Preparative scale electrolysis experiments are referenced vs. SCE (Fc$^+$/Fc redox couple at +0.5 V vs. SCE).

H$_2$ detection was performed using the method described by Summers *et al.* in reference 29. Briefly, **CuTFcP** and **PdTFcP** (0.1 mM), solutions in DMF containing TFA (50 mM) and TBABF$_4$ (0.2 M), were prepared from thoroughly degassed stock solutions and stored under Ar. Ar was continually flowed through the solution and into a 6 port 2 position switch (VICI) at a constant

flow (typically 10 cm^3 min^{-1}), maintained using a mass flow controller (Bronkhorst, E-Flow series). A 200 µL sample was analyzed automatically every 3 min using a gas chromatograph (Shimadzu 2014) with a thermal conductivity detector operating at 50 °C. The sample was initially passed through a dry ice trap to remove any condensable solvents. Ar was used as the carrier gas and H$_2$ was detected on an activated molecular sieve column (Shincarbon ST, Restek). Integration of a plot of the production rate versus time yields the total amount of H$_2$ produced. A voltage was applied using an IVIUMSTAT potentiostat, a glassy carbon working electrode, platinum wire counter electrode and a saturated calomel reference electrode.

Computational calculations were performed using a 32-bit version of Gaussian09 on a quadruple-core Intel Xeon system with 4GB RAM. The calculations were run in parallel, fully utilising the multi-core processor. Structures were firstly minimised at the Hartree-Fock level and the generated geometries were used to feed the DFT calculations. Energy minimization calculations were monitored using the programme Molden and run in parallel with frequency calculations to ensure optimized geometries represented local minima. An optimised structure for the anion was calculated starting from the neutral form as a doublet state; the dianion structure was subsequently calculated from the anion form at the singlet level.

All chemicals were purchased from commercial sources and used as received unless otherwise stated. Basic solvents for synthesis were dried using literature methods. Solvents for spectroscopic investigations were of the highest purity available. Compounds **H₂TFcP**,[18] **CuTFcP**,[20] **CuTPP**[45] and **PdTPP**[46] were prepared by the literature procedures.

Preparation of Palladium(II) 5,10,15,20-tetraferrocenyl porphyrin PdTFcP

A solution of Pd(OAc)$_2$ (85 mg, 0.38 mmol, 2 eq) and **H₂TFcP** (200 mg, 0.19 mmol) in toluene (25 mL) was refluxed under N$_2$ in darkness until the TLC analysis indicated that all starting material was consumed (20 h). The reaction mixture was washed with distilled water (3 x 30 mL), the organic phase dried over anhydrous Na$_2$SO$_4$, filtered, concentrated and the residue was eluted with toluene on a silica gel column to obtain **PdTFcP** (43 mg, 20%) as a purple microcrystalline powder. ^{1}H-NMR (400 MHz, CDCl$_3$, ppm): δ 9.67 (s, 8H, β-pyrrole), 5.27 (ap t, J = 1.8 Hz, 8H, α-Cp), 4.74 (ap t, J = 1.8 Hz, 8H, β-Cp), 3.98 (s, 20H, CpH). ^{13}C NMR (101 MHz, CDCl$_3$, ppm): δ 140.9 (α-pyrrole), 131.2 (β-pyrrole), 119.0 (C$_{meso}$), 89.3 (Cp$_{ipso}$), 76.7 (α-Cp, solvent overlap), 70.5 (CpH), 69.0 (β-Cp). UV-Vis (THF): λ$_{max}$, nm (ε, 10^3 mol^{-1} cm^{-1}): 324 (17), 431 (66), 490 (sh), 654 (14). MS (MALDI-TOF, DCTB matrix, m/z): calcd. (fnd.) for C$_{60}$H$_{44}$Fe$_4$N$_4$Pd: 1150.0 (1150.0) [M]$^+$. Elemental analysis calcd. for C$_{60}$H$_{44}$Fe$_4$N$_4$Pd · 1/3C$_6$H$_5$CH$_3$ C 63.37, H 3.98, N 4.74, fnd. C 63.84, H 4.04, N 4.76. (Note: the small trace of toluene is also evident in the ^{1}H-NMR spectrum, thus accounting for the high carbon content).

Notes and references

1. A. J. Bard and M. A. Fox, *Acc. Chem. Res.,* 1995, **28**, 141.
2. N. S. Lewis, D. G. Nocera, *PNAS*, 2006, **103**, 15729.
3. J. D. Holladay, D. L. Hu and Y. King Wang *Catal. Today* 2009. **139**, 244.
4. C. Koroneos, A. Dompros, G. Roumbas and N. Moussiopoulos, *Int. J. Hydrogen Energ.,* 2004, **29**, 1443.
5. M. Carmo, D. L. Fritz, J. Mergel and D. A Stolten, *Int. J. Hydrogen Energ.,* 2013, **38**, 4901.
6. M. Gong, W. Zhou, M.-C. Tsai, J. Zhou, M. Guan, M.-C. Lin, B. Zhang, Y. Hu, D.-Y. Wang, J. Yang, S. J. Pennycook, B.-J. Hwang and H. Dai, *Nature Commun.,* 2014, **5**, 4695.
7. A. J. Appleby, G. Crepy and J. Jacquelin, *Int. J. Hydrogen Energ.,* 1978, **3**, 21.
8. X. Hu, B. S. Brunschwig and J. C. Peters, *J. Am. Chem. Soc.,* 2007, **129**, 8988.
9. N. Phougat, P. Vasudevan, K. M. Jha and D. K. Bandhopadhyay, *Trans. Met. Chem.,* 2003, **28**, 838.
10. J. Y. Becker, B. Vainas, R. Eger and L. Kaufman, *J. Chem. Soc., Chem. Commun.,* 1985, 1471.
11. K. Takahashi, K. Hiratsuka, H. Sasaki and S. Toshima, *Chem. Lett.,* 1979, **8**, 305.
12. I. Bhugun, D. Lexa and J.-M. Savéant, *J. Phys. Chem.,* 1996, **100**, 19981.
13. R. M. Kellett and T. G. Spiro, *Inorg. Chem.,* 1985, **24**, 2373; C. H. Lee, D. K. Dogutan, and D. G. Nocera. *J. Am. Chem. Soc.* 2011, **133**, 8775; B. Mondal, K. Sengupta, A. Rana, A. Mahammed, M. Botoshansky, S. Ghosh Dey, Z. Gross and A. Dey. *Inorg. Chem.,* 2013, **52**, 3381; A. Mahammed, B. Mondal, A. Rana, A. Dey and Z. Gross. *Chem. Commun.,* 2014, **50**, 2725.
14. I. Bhugun, D. Lexa and J.-M. Savéant, *J. Am. Chem. Soc.,* 1996, **118**, 3982.
15. J. Chu, X.-H. Xie, S,-R. Yang and S.-Z. Zhan. *Inorg. Chim. Acta*, 2014, **410**, 191.
16. S. Samanta, K. Sengupta, K. Mittra, S. Bandyopadhyay and A. Dey, *Chem. Commun.,* 2012, **48**, 7631; K. Mittra, S. Chatterjee, S. Samanta and A. Dey, *Inorg. Chem.,* 2013, **52**, 14317.
17. B. Sun, Z. Ou, D. Meng, Y. Fang, Y. Song, W. Zhu, P. V. Solntsev, V. N. Nemykin and K. M. Kadish, *Inorg. Chem.,* 2014, **53**, 8600.
18. N. M. Loim, N. V. Abramova and V. I. Sokolov, *Mendeleev Commun.,* 1996, 46.
19. S. J. Narayanan, S. Venkatraman, S. R. Dey, B. Sridevi, V. R. G. Anand and T. K. Chandrashekar, *Synlett,* 2000, 1834.
20. V. N. Nemykin, P. Galloni, B. Floris, C. D. Barrett, R. G. Hadt, R. I. Subbotin, A. G. Marrani, R. Zanonic and N. M. Loim, *Dalton Trans.,* 2008, 4233.
21. G. T. Rohde, J. R. Sabin, C. D. Barrett and V. N. Nemykin, *New J. Chem.,* 2011, **35**, 1440.
22. V. N. Nemykin and R. G. Hadt, *J. Phys. Chem. A,* 2010, **114**, 12062.
23. V. N. Nemykin, P. Chen, P. V. Solntsev, A. A. Purchel and K. M. Kadish, *J. Porphyr. Phthalocya.*, 2012, **16**, 793.

24 G. L. Closs and L. E. Closs, *J. Am. Chem. Soc.,* 1963, **85**, 818; J. G. Lanese and G. S. Wilson, *J. Electrochem. Soc.,* 1972, **119**, 1039.

25 G. S. Wilson and G. Peychal-Heiling, *Anal. Chem.,* 1971, **43** 550.

26 V. N. Nemykin, G. T. Rohde, C. D. Barrett, R. G. Hadt, J. R. Sabin, G. Reina, P. Galloni and B. Floris, *Inorg. Chem.,* 2010, **49**, 7497; V. N. Nemykin, G. T. Rohde, C. D. Barrett, R. G. Hadt, C. Bizzarri, P. Galloni, B. Floris, I. Nowik, R. H. Herber, A. G. Marrani, R. Zanoni and N. M. Loim, *J. Am. Chem. Soc.,* 2009, **131**, 14969.

27 V. Fourmond, P.-A. Jacques, M. Fontecave and V. Artero, *Inorg. Chem.,* 2010, **49**, 10338.

28 V. Artero and J.-M. Saveant. *Energy Environ. Sci.,* 2014, **7**, 3808.

29 P. A. Summers, J. Dawson, F. Ghiotto, M. W. D. Hanson-Heine, K. Q. Vuong, E. S. Davies, X.-Z. Sun, N. A. Besley, J. McMaster, M. W. George and M. Schröder, *Inorg. Chem.,* 2014, **53**, 4430.

30 V. Fourmond, S. Canaguier, B. Golly, M. J. Field, M. Fontecaveac and V. Artero, *Energy Environ. Sci.,* 2011, **4**, 2417.

31 B. Krattinger and H. J. Callot *Chem. Commun.,* 1996, 1341.

32 J.-M. Savéant, *Energy Environ. Sci.,* 2012, **5**, 7718.

33 Y. Fang, P. Bhyrappa, Z. Ou and K. M. Kadish, *Chem. Eur. J.,* 2014, **20**, 524.

34 M. J. Frisch, G. W. Trucks, H. B. Schlegel, G. E. Scuseria, M. A. Robb, J. R. Cheeseman, J. A. Montgomery, Jr., T. Vreven, K. N. Kudin, J. C. Burant, J. M. Millam, S. S. Iyengar, J. Tomasi, V. Barone, B. Mennucci, M. Cossi, G. Scalmani, N. Rega, G. A. Petersson, H. Nakatsuji, M. Hada, M. Ehara, K. Toyota, R. Fukuda, J. Hasegawa, M. Ishida, T. Nakajima, Y. Honda, O. Kitao, H. Nakai, M. Klene, X. Li, J. E. Knox, H. P. Hratchian, J. B. Cross, V. Bakken, C. Adamo, J. Jaramillo, R. Gomperts, R. E. Stratmann, O. Yazyev, A. J. Austin, R. Cammi, C. Pomelli, J. W. Ochterski, P. Y. Ayala, K. Morokuma, G. A. Voth, P. Salvador, J. J. Dannenberg, V. G. Zakrzewski, S. Dapprich, A. D. Daniels, M. C. Strain, O. Farkas, D. K. Malick, A. D. Rabuck, K. Raghavachari, J. B. Foresman, J. V. Ortiz, Q. Cui, A. G. Baboul, S. Clifford, J. Cioslowski, B. B. Stefanov, G. Liu, A. Liashenko, P. Piskorz, I. Komaromi, R. L. Martin, D. J. Fox, T. Keith, M. A. Al-Laham, C. Y. Peng, A. Nanayakkara, M. Challacombe, P. M. W. Gill, B. Johnson, W. Chen, M. W. Wong, C. Gonzalez, J. A. Pople, Gaussian 03, Gaussian, Inc., Wallingford CT, 2004.

35 S. Fu, X. Zhu, G. Zhou, W.-Y. Wong, C. Ye, W.-K. Wong and Z. Li, *Eur. J. Inorg. Chem.,* 2007, 2004.

36 Y. Cho, J.H. Lee, J. Jaworski, S. Park, S. S. Lee and J. H. Jung, *New J. Chem.,* 2012, **36**, 32.

37 T. P. G. Sutter, R. Rahimi, P. Hambright, J. C. Bommer, M. Kumar and P. Neta, *J. Chem. Soc., Faraday Trans.,* 1993, **89**, 495.

38 V. N. Nemykin, G. T. Rohde, C. D. Barrett, R. G. Hadt, J. R. Sabin, G. Reina, P. Galloni and B. Floris, *Inorg. Chem.,* 2010, **49**, 7497.

39 P. V. Solntsev B.D. Neisen, J.R. Sabin, N.N. Gerasimchuk and V. N. Nemykin, *J. Porphyr. Phthalocya.*, 2011, **15**, 612; S. J. Dammer, P. V. Solntsev, J. R. Sabin and V. N. Nemykin, *Inorg. Chem.,* 2013, **52**, 9496.

40 E. E. Bonfantini, A. K. Burrell, W. M. Campbell, M. J. Crossley, J. J. Gosper, M. M. Harding, D. L. Officer and D. C. W. Reid, *J. Porphyr. Phthalocya.*, 2002, **6**, 708.

41 A. C. Benniston, D. Sirbu, C. Turta, M. R. Probert, W. Clegg, *Tetrahedron Lett.,* 2014, **55**, 3777.

42 C. Costentin, M. Robert and J.-M. Savéant, *J. Am. Chem. Soc.,* 2006, **128**, 8726.

43 C. Costentin, M. Robert, J.-M. Savéant and A.-L. Teillout, *PNAS*, 2009, **106**, 11829.

44 B. H. Solis, A. G. Maher, T. Honda, D. C. Powers, D. G. Nocera and S. Hammes-Schiffer, *ACS Catal.,* 2014, **4**, 4516.

45 W. M. Campbell, K. W. Jolley, P. Wagner, K. Wagner, P. J. Walsh, K. C. Gordon, L. Schmidt-Mende, M. K. Nazeeruddin, Q. Wang, M. Gratzel and D. L. Officer, *J. Phys. Chem. C*, 2007, **111**, 11760.

46 A. Gabrielsson, J. R. L. Smith and R. N. Perutz, *Dalton Trans.*, 2008, 4259.